TAGGED CARDIAC MR IMAGE SEGMENTATION USING BOUNDARY & REGIONAL-SUPPORT AND GRAPH-BASED DEFORMABLE PRIORS

Bo Xiang[1,2]*, Chaohui Wang*[1,2]*, Jean-Francois Deux*[3]*, Alain Rahmouni*[3]*, Nikos Paragios*[1,2]

[1] Laboratoire MAS, Ecole Centrale de Paris, France
[2] Equipe GALEN, INRIA Saclay - Île de France, Orsay, France
[3] Radiology Department, Henri Mondor Hospital, Créteil, France

ABSTRACT

Segmentation and tracking of tagged MR images is a critical component of in vivo understanding for the heart dynamics. In this paper, we propose a novel approach which uses multi-dimensional features and casts the left ventricle (LV) extraction problem as a maximum posteriori estimation process in both the feature and the shape spaces. Exact integration of multi-dimensional boundary and regional statistics is achieved through a global formulation. Prior is enforced through a point-distribution model, where distances between landmark positions are learned and enforced during the segmentation process. The use of divergence theorem leads to an elegant pairwise formulation where image support and prior knowledge are jointly encoded within a pairwise MRF and the segmentation is achieved efficiently by employing MRF inference algorithms. Promising results on numerous examples demonstrate the potentials of our method.

Index Terms— Tagged MR images, Segmentation, Shape Prior, Markov Random Fields, Divergence Theorem

1. INTRODUCTION

MR-tagging is a modality offering important potentials on the diagnosis of cardio-vascular diseases. Segmentation, tracking and in particular motion strain are important features which can be determined from image sequences and are valuable indicators to assess the heart's state. On the other hand, these images are often of low resolution and the extraction of the myocardial boundaries is far from being trivial. This has been addressed through the integration of feature extraction and segmentation methods (e.g. [1, 2]).

Deformable contours/surfaces and templates [3] are among the most commonly used methods for tagged MR image segmentation. The use of "homogeneity" hypothesis in an appropriate feature space is often considered to separate the left ventricle (LV) from the myocardium, the right ventricle and the remaining anatomical features. Gabor features [4] using various number of scales and orientations, wavelets [5], and co-occurrence matrices are examples of feature spaces. These features are fed to a segmentation algorithm that often combines them with prior knowledge. The use of active contours and deformable surfaces [6, 3] are among the most popular methods to perform knowledge-based segmentation. The segmentation is solved by seeking a deformation of an initial contour in the image plane towards optimal "feature" separation of the myocardium from the left ventricle while being constrained to be part of a learned manifold. The use of boundary features is quite problematic due to the texture nature of images imposed from the tagging, unless proper edge detectors are defined. Such an approach exhibits two important limitations. The first is inherited from the continuous formulation of the active contour/surface nature which makes the recovery of the optimal solution an intractable task. The second is with the construction of the prior manifold that often requires a significant number of samples due to the dimensionality of the representation.

In this paper, we propose a novel approach to address the above mentioned limitations. Firstly, we propose a graphical representation [7] to model the LV shape, where the manifold is constructed by accumulating local constraints on the relative positions of points. Secondly, based on this representation, we develop a global approach to jointly encode regional statistics, boundary support, as well as prior knowledge on the shape within a probabilistic framework, towards optimal separation between the LV and the remaining anatomical structures. The proposed exact factorization of the regional data term leads to an elegant pairwise MRF segmentation formulation which jointly models both the shape prior and the data likelihood. Finally, by employing Gabor features as the cues from the image support and efficient MRF inference algorithms such as Fast-PD [8], our method has been demonstrated by experiments to be able to achieve highly accurate performance with a very fast computational speed.

The reminder of this paper is organized as follows: In section 2 we discuss the mathematical foundations of our method. Its discrete variant and the corresponding MRF formulation are presented in section 3. Experimental results are part of section 4, while discussion concludes the paper in section 5.

2. PROBABILISTIC FRAMEWORK

One of the most interesting structures in the cardiac image analysis is the myocardium structure, which is the muscle between the endocardium and the epicardium. The extraction of this structure can lead to the estimation of blood volume, the wall strain motion, etc., which are important diagnostic measurements. This is particularly the case when referring to tagged MR images where a pattern has been introduced in the acquisition, making the segmentation task more complex due to the resolution, texture and noise. In such a context, we aim to partition the image domain Ω into three segments (Fig. 1(a)): (1) the endocardium Ω_e; (2) the myocardium $\Omega_m = \Omega_o - \Omega_e$; (3) the background $\Omega_b = \Omega - \Omega_o$, where $\Omega_o = \Omega_e \cup \Omega_m$. Obviously, Ω_e, Ω_m and Ω_b should satisfy the following conditions: (i) Each of them is connected; (ii) They are mutually disjointed; (iii) Their union is the whole image domain. Thus, for the joint variable $\mathbf{\Omega} = (\Omega_e, \Omega_m, \Omega_b)$, we define the space dom($\mathbf{\Omega}$) as the set of all the possible combinations of Ω_e, Ω_m and Ω_b that satisfy the above three constraints.

Knowledge-based image segmentation aims to partition the image domain by searching for a compromise between data-attraction and shape-fitness with the prior model, and can be formulated as a maximization of the posterior probability (MAP) of $\mathbf{\Omega}$ over the space dom($\mathbf{\Omega}$):

$$\mathbf{\Omega}^{\text{opt}} = \arg \max_{\mathbf{\Omega} \in \text{dom}(\mathbf{\Omega})} p(\mathbf{\Omega}|\mathbf{I}) \tag{1}$$

where:

$$p(\mathbf{\Omega}|\mathbf{I}) = \frac{p(\mathbf{\Omega}, \mathbf{I})}{p(\mathbf{I})} \propto p(\mathbf{\Omega}, \mathbf{I}) = p(\mathbf{I}|\mathbf{\Omega}) \cdot p(\mathbf{\Omega}) \tag{2}$$

Here, $p(\mathbf{I}|\mathbf{\Omega})$ encodes the data likelihood of the image $\mathbf{I}$ given the segmentation $\mathbf{\Omega}$, and $p(\mathbf{\Omega})$ encodes the prior knowledge on the segmentation. The data term is seeking for discontinuities while optimally separating the statistical properties of the three populations. Complementary to that, the shape prior term constrains the segmentation solution to be part of a learned manifold and imposes smoothness on the extracted boundary.

2.1. Data Likelihood

We combine the region-based and boundary-based data likelihoods within the proposed formulation towards a better performance [9]. To this end, we model the likelihood $p(\mathbf{I}|\mathbf{\Omega})$ as follows:

$$p(\mathbf{I}|\mathbf{\Omega}) = \frac{1}{Z} \cdot \exp\{-E_{\text{data}}(\mathbf{I}, \mathbf{\Omega})\} \tag{3}$$

where $\mathbf{I}$ denotes an image of features (such as intensity values, Gabor features, Wavelet coefficients, etc.), Z is a normalizing constant, and the energy function $E_{\text{data}}(\mathbf{I}, \mathbf{\Omega})$ is defined as:

$$E_{\text{data}}(\mathbf{I}, \mathbf{\Omega}) = \lambda_1 E^{(1)}_{\text{data}}(\mathbf{I}, \mathbf{\Omega}) + \lambda_2 E^{(2)}_{\text{data}}(\mathbf{I}, \mathbf{\Omega}) \tag{4}$$

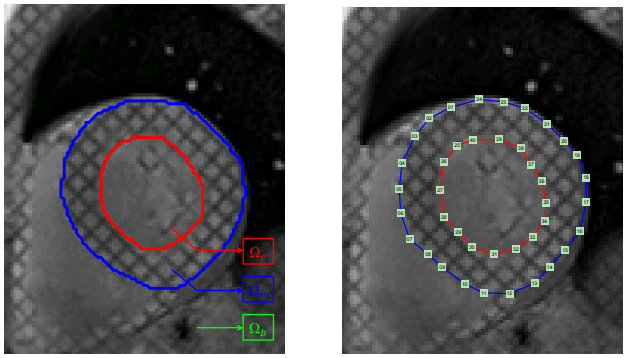

(a) (b)

Fig. 1. (a) Tagged Cardiac MRI with manual segmentation. (b) Distribution of the control points in the shape model.

where $\lambda_1 > 0$ and $\lambda_2 > 0$ are two weight coefficients, $E^{(1)}_{\text{data}}$ denotes the regional term which encodes the statistical properties of the three populations, and $E^{(2)}_{\text{data}}$ denotes the boundary term which encodes discontinuities along the boundaries. The two data terms are defined as follows:

$$\begin{aligned} E^{(1)}_{\text{data}}(\mathbf{I}, \mathbf{\Omega}) &= \iint_{\Omega_e} -\log p_e(I(x,y)) + \iint_{\Omega_m} -\log p_m(I(x,y)) \\ &+ \iint_{\Omega_b} -\log p_b(I(x,y)) \\ &= \iint_{\Omega_e} \log \frac{p_m(I(x,y))}{p_e(I(x,y))} + \iint_{\Omega_e \cup \Omega_m} \log \frac{p_b(I(x,y))}{p_m(I(x,y))} \\ &+ \iint_{\Omega_e \cup \Omega_m \cup \Omega_b} -\log p_b(I(x,y)) \\ &= \iint_{\Omega_e} \log \frac{p_m(I(x,y))}{p_e(I(x,y))} + \iint_{\Omega_o} \log \frac{p_b(I(x,y))}{p_m(I(x,y))} \\ &+ \text{constant} \end{aligned} \tag{5}$$

and

$$E^{(2)}_{\text{data}}(\mathbf{I}, \mathbf{\Omega}) = \oint_{\partial\Omega_e} -\log p^{(1)}_d(I(x,y)) + \oint_{\partial\Omega_o} -\log p^{(2)}_d(I(x,y)) \tag{6}$$

where $I(x,y)$ denotes the feature vector at location (x,y), $\partial\Omega_e$ and $\partial\Omega_o$ denote the boundaries which correspond to the endocardium and the epicardium respectively, $p^{(1)}_d$ and $p^{(2)}_d$ denote the corresponding discontinuity probabilities, p_e, p_m and p_b denote the distributions of the features for the regions of the endocardium, the myocardium and the background respectively. We can assume that the discontinuity probability is independent of the transition between classes, but such an assumption can be amended as well by employing class specific transition probabilities.

To deal with the tagged MR images, we use Gabor features [4] as the image features instead of the intensities, due to their abilities to capture micro and macro-texture in different scales and orientations. Thus each pixel has a multi-resolution representation given a number of scales and a number of orientations. Regarding the boundary probability, we can consider the transition map between texture classes as suggested in [9].

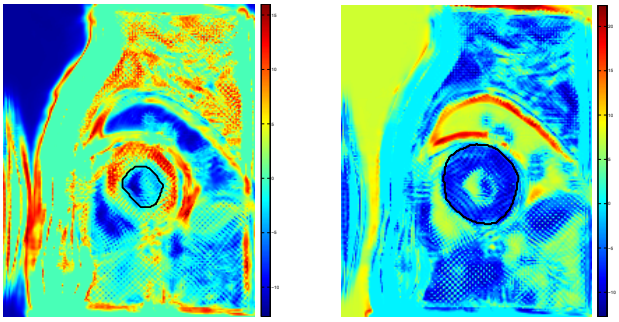

(a) $\log p_m - \log p_e$ (b) $\log p_b - \log p_m$

Fig. 2. Image of likelihoods using Gabor features.

Given the feature space, Gaussian Mixture Models (GMMs) are used to model each of the distributions of the three regions of interest. Their distributions can be learned from training data using standard methods such as Expectation Maximization (EM) with Bayesian Information Criterion (BIC) [10]:

$$p_r(I) = \sum_{k=1}^{K_r} \pi_r^k \mathcal{N}(I|\boldsymbol{\mu}_r^k, \boldsymbol{\Sigma}_r^k), \quad r \in \{e, m, b\} \qquad (7)$$

where for segment r, K_r denotes the number of Gaussian components, $\mathcal{N}(I|\boldsymbol{\mu}_r^k, \boldsymbol{\Sigma}_r^k)$ denotes a component k with mean $\boldsymbol{\mu}_r^k$ and covariance matrix $\boldsymbol{\Sigma}_r^k$, and π_r^k denotes the mixing coefficient of component k. Fig. 2 shows the results on a test image, where we plot the ground truth boundaries corresponding to the endocardium (in Fig. 2(a)) and the epicardium (in Fig. 2(b)) to show the quality of the likelihoods.

Given the visual support, the next step consists of modeling prior knowledge with respect to the geometric manifold of allowable shape variations.

2.2. Point-distribution Shape Model

One key problem of knowledge-based segmentation is how to encode prior information using a compact representation which can be easily adopted towards efficient segmentation. We use a point-distribution model due to its advantages such as: (1) the ability to describe both the generality and the variability of the object of interest; (2) be easily encoded in an MRF model which can fuse data term and prior term in a principled way and lead to an efficient optimization solution.

The myocardium structure in a 2D image is bounded by two boundaries $\boldsymbol{\mathcal{C}} = (\mathcal{C}_e, \mathcal{C}_o)$, where $\mathcal{C}_e = \partial\Omega_e$ and $\mathcal{C}_o = \partial\Omega_O$ correspond to the endocardium and the epicardium respectively.

We model a boundary using a number (16 for $\mathcal{C}_e$ and 24 for $\mathcal{C}_o$) of control points which are located on the boundary (Fig. 1(b)). Let us take $\mathcal{C}_e$ for example. $\mathcal{V}_e = \{1, 2, \ldots, N\}$ denotes the index set of the control points. The control points are endowed 2D coordinates $u_i = (x_i, y_i)$ $(i \in \mathcal{V}_e)$, and are indexed counter-clockwise along the boundary such that point i and j are neighbors if $(i,j) \in \mathcal{E}_e^C = \{(i,j)|i,j \in \mathcal{V}_e \text{ and } j\%N = (i+1)\%N\}$, where "%" denotes the modulo operator. Without loss of generality, we use linear interpolation based on the position of the control points to model the boundary and obtain the boundary model $\mathcal{C}_e(\mathbf{u}_e)$ which consists of the line segments between these neighbor control points, i.e., $\mathcal{C}_e(\mathbf{u}_e) = \{\vec{u_i u_j} \ |(i,j) \in \mathcal{E}_e^C\}$, where $\mathbf{u}_e = (u_i)_{i \in \mathcal{V}_e}$. Similarly, we can define the counterparts $\mathcal{V}_o$, $\mathcal{E}_o^C$, $\mathbf{u}_e$ and $\mathcal{C}_o(\mathbf{u}_o)$ for $\mathcal{C}_o$.

We aim to use the statistics on the Euclidean distances $d_{ij} = \|u_i - u_j\|$ between a pair (i,j) of control points to model the shape [7]. Due to the movement of heart, the scale/length of the boundaries can vary significantly and therefore it has to be taken into account during modeling. On the other hand, the distance between the epicardium and the endocardium relative position boundaries is less important. In order to characterize the shape well, we propose to use two different models to encode these two types of priors.

Since the variation of the boundaries is scale-related, like [7], we use the normalized distance $\hat{d}_{ij}$ to achieve a similarity-invariant shape model:

$$\hat{d}_{ij} = \frac{d_{ij}}{\frac{1}{N_r}\sum_{(i,j)\in\mathcal{E}_r} d_{ij}} \qquad (8)$$

where $\mathcal{E}_r = \{(i,j)|i,j \in \mathcal{V}_r \text{ and } i \neq j\}$ denotes the set (all the combinations) of pairs of points for the boundary $\mathcal{C}_r$ $(r \in \{e,o\})$, and N_r is the cardinal of $\mathcal{E}_r$, i.e., the number of pairs of points. By aligning the boundaries in the given M training data, we learn a Gaussian Mixture to model the distribution p_{ij} $((i,j) \in \mathcal{E}_e \cup \mathcal{E}_o)$ of the normalized distance between each pair of points.

A similar method is adopted for the interactions between epicardium and endocardium without scale being taken into account. The statistics of this interaction are learned directly on the distance between a point i from the boundary $\mathcal{C}_e$ and a point j from the boundary $\mathcal{C}_o$ to model the geometry constraints between the two boundaries. Importantly, such prior can avoid the intersection of the two boundaries. We also use Gaussian Mixtures to model the distributions p_{ij} $((i,j) \in \mathcal{E}_{int} = \mathcal{V}_e \times \mathcal{V}_o)$ of the distances.

The prior probability on the shape configuration can be defined as follows:

$$p(\boldsymbol{\Omega}(\mathbf{u})) = p(\mathbf{u}) = \frac{1}{Z'} \cdot \prod_{(i,j)\in\mathcal{E}_e\cup\mathcal{E}_o} p_{ij}(\hat{d}_{ij}) \cdot \prod_{(i,j)\in\mathcal{E}_{int}} p_{ij}(d_{ij}) \qquad (9)$$

where Z' is a normalizing constant, and $\boldsymbol{\Omega}(\mathbf{u})$ denotes the mapping from the positions $\mathbf{u} = \mathbf{u}_e \cup \mathbf{u}_o$ of all the control points to the configuration of the three segments. Within such a framework, we can further integrate the smoothness prior using higher-order interaction.

3. MARKOV RANDOM FIELD FORMULATION

In this section, we reformulate the above probabilistic framework within a pairwise MRF, so that we can employ the recently developed MRF inference algorithms such as Fast-PD [8] and TRW-S [11] to achieve a good optimum with a very fast speed.

To this end, we use a node to model a control point and an edge to model the interaction between a pair of points. Let $\mathcal{V} = \mathcal{V}_e \cup \mathcal{V}_o$ denote the set of nodes, and $\mathcal{E} = \mathcal{E}_e \cup \mathcal{E}_o \cup \mathcal{E}_{int}$ the set of edges. Each node i ($i \in \mathcal{V}$) is associated with a latent variable U_i which corresponds to the position configuration u_i of the corresponding control point. Let $\mathcal{U}_i$ denote the candidate space for the configuration u_i of node i. With such an MRF, the segmentation (Eq. 1) can be reformulated as the inference of the configuration $\mathbf{u} = (u_i)_{i\in\mathcal{V}}$ of all the nodes over the candidate space $\mathcal{U} = \prod_{i\in\mathcal{V}} \mathcal{U}_i$:

$$\mathbf{u}^{\text{opt}} = \arg\min_{\mathbf{u}\in\mathcal{U}} E(\mathbf{u}) \tag{10}$$

where the energy $E(\mathbf{u})$ is defined as the negative logarithm of the posterior probability $p(\mathbf{\Omega}(\mathbf{u})|\mathbf{I})$ (Eq. 2) minus a constant:

$$E(\mathbf{u}) = -\log p(\mathbf{I}|\mathbf{\Omega}(\mathbf{u})) - \log p(\mathbf{\Omega}(\mathbf{u})) \tag{11}$$

3.1. Exact Data Likelihood Factorization

While the prior term $-\log p(\mathbf{\Omega}(\mathbf{u}))$ (Eq. 9) and the boundary data term $E^{(2)}_{\text{data}}(\mathbf{I}, \mathbf{\Omega}(\mathbf{u}))$ (Eq. 6) can be easily factorized within a pairwise MRF, the factorization of the regional data likelihood $E^{(1)}_{\text{data}}(\mathbf{I}, \mathbf{\Omega}(\mathbf{u}))$ (Eq. 5) is much more difficult since it involves integrals on the regions which are delimited by the contour depending on the positions of all the control points. An approximation of this data term based on Voronoi-decomposition was proposed in [7]. However, we show that this data term can be exactly factorized within a pairwise MRF, which leads to significantly better results (see comparison in section 4). We present below the proposed exact factorization of the regional likelihood by using *Divergence Theorem*.

The 2D-divergence theorem (in 2D, it is also known as Green's Theorem) states the equivalence between a line integral around a simple closed curve $\mathcal{C}$ and a double integral over the plane region $\mathcal{D}$ bounded by $\mathcal{C}$:

$$\iint_{\mathcal{D}} \text{div}\mathbf{F} dxdy = \oint_{\mathcal{C}} \mathbf{F}\cdot\ \vec{\mathbf{n}}\ ds \tag{12}$$

where $\mathbf{F} = (F_x, F_y)$, $\text{div}\mathbf{F} = \frac{\partial F_x}{\partial x} + \frac{\partial F_y}{\partial y}$ and $\vec{\mathbf{n}} = \mathbf{i}\frac{dy}{ds} - \mathbf{j}\frac{dx}{ds}$ denotes the outward-pointing unit normal to $\mathcal{C}$. Let us choose $F_y = 0$, then:

$$\iint_{\mathcal{D}} \frac{\partial F_x}{\partial x} dxdy = \oint_{\mathcal{C}} F_x dy \tag{13}$$

To associate the divergence theorem with the computation of $E^{(1)}_{\text{data}}$, let $\frac{\partial G^{(1)}(x,y)}{\partial x} = \log\frac{p_m(I(x,y))}{p_e(I(x,y))}$, and $\frac{\partial G^{(2)}(x,y)}{\partial x} = \log\frac{p_b(I(x,y))}{p_m(I(x,y))}$. By assuming the probabilities are all equal outside the image, we obtain:

$$\begin{cases} G^{(1)}(x,y) = \int_0^x \log\frac{p_m(I(t,y))}{p_e(I(t,y))} dt \\ G^{(2)}(x,y) = \int_0^x \log\frac{p_b(I(t,y))}{p_m(I(t,y))} dt \end{cases} \tag{14}$$

In accordance with the divergence theorem (Eq. 12), we transfer the regional data term into integrals of $G^{(1)}$ and $G^{(2)}$ on the corresponding boundaries, and then factorize it into the sum of integrals on the directional segments that compose the boundaries:

$$\begin{aligned} E^{(1)}_{\text{data}}(\mathbf{I}, \mathbf{\Omega}(\mathbf{u})) &= \oint_{\mathcal{C}_e(\mathbf{u})} G^{(1)}(x,y)dy + \oint_{\mathcal{C}_o(\mathbf{u})} G^{(2)}(x,y)dy \\ &= \sum_{(i,j)\in\mathcal{E}_e^C} \int_{\overrightarrow{u_i u_j}} G^{(1)} dy + \sum_{(i,j)\in\mathcal{E}_o^C} \int_{\overrightarrow{u_i u_j}} G^{(2)} dy \end{aligned} \tag{15}$$

Furthermore, the computation of this data term can be done very efficiently. We present the detail of the numeric computation in Appendix.

3.2. Factorized Energy

Following the above derivation, we factorize the energy exactly within a pairwise MRF. The energy can be written as:

$$\begin{aligned} E(\mathbf{u}) = &\sum_{(i,j)\in\mathcal{E}_e^C} \psi^{(1)}_{ij}(u_i,u_j) + \sum_{(i,j)\in\mathcal{E}_o^C} \psi^{(2)}_{ij}(u_i,u_j) \\ &+ \sum_{(i,j)\in\mathcal{E}_e\cup\mathcal{E}_o} \psi^{(3)}_{ij}(u_i,u_j) + \sum_{(i,j)\in\mathcal{E}_{int}} \psi^{(4)}_{ij}(u_i,u_j) \end{aligned} \tag{16}$$

where $\psi^{(1)}$ and $\psi^{(2)}$ encode the data likelihood, while $\psi^{(3)}$ and $\psi^{(4)}$ encode the shape prior. They are defined as follows:

$$\begin{cases} \psi^{(1)}_{ij}(u_i,u_j) = \lambda'_1 \cdot \int_{\overrightarrow{u_i u_j}} G^{(1)}(x,y)dy - \lambda'_2 \cdot \int_{\overrightarrow{u_i u_j}} \log p^{(1)}_d(I(x,y))ds \\ \psi^{(2)}_{ij}(u_i,u_j) = \lambda'_1 \cdot \int_{\overrightarrow{u_i u_j}} G^{(2)}(x,y)dy - \lambda'_2 \cdot \int_{\overrightarrow{u_i u_j}} \log p^{(2)}_d(I(x,y))ds \\ \psi^{(3)}_{ij}(u_i,u_j) = -\log p_{ij}(\hat{d}_{ij}) \\ \psi^{(4)}_{ij}(u_i,u_j) = -\log p_{ij}(d_{ij}) \end{cases} \tag{17}$$

where $\lambda'_1 > 0$ and $\lambda'_2 > 0$ are two weight coefficients.

Given an initial configuration of the myocardium, for each control point i, we sample uniformly in the neighborhood centered at its position to get the candidate set $\mathcal{U}_i$ [12]. Given such a label space, the optimal solution is achieved through the MRF inference. Then we consider it as a new start position of the myocardium and estimate the current scales of the boundaries. This step is repeated until there is no more changes on the position configuration of the control points.

4. EXPERIMENTAL RESULTS

We validate our method on a dataset which consists of 60 tagged cardiac MR images. Standard of reference was

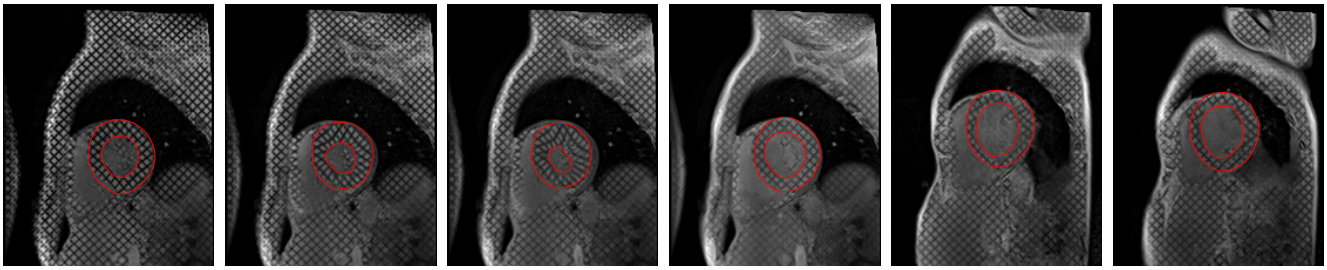

Fig. 3. Segmentation results on different test images using the same initialization. The contours in red represent the obtained boundaries that partition the image into three segments.

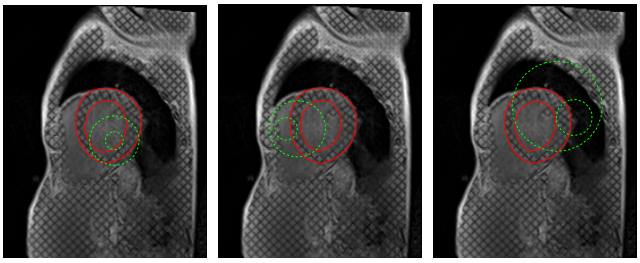

(a) (b) (c)

Fig. 4. Segmentation results with different initializations. The contours in red represent the obtained boundaries, while the contours in green represent the initialization of the shape model.

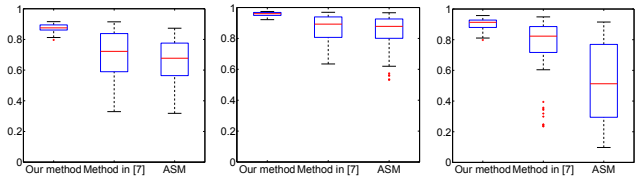

(a) Endocardium Ω_e (b) Epicardium Ω_o (c) Myocardial Ω_m

Fig. 5. Boxplots of the Dice coefficients. Each sub-figure presents three boxes corresponding to the Dice coefficients on the segmentation of a region of interest, obtained by our method, the one in [7] and standard ASM method, respectively. In each box, the central mark in red is the median, the edges of the box are the 25th and 75th percentiles.

available, consisting of annotations of epicardium and endocardium boundaries provided by experts. These MR images were acquired by a 3-T Siemens MR imaging system equipped with a high-performance gradient system (maximum amplitude: 40 mT/m; minimum rise: slew rate 200 mT.m^{-1}/s) using a 32-channel phased-array cardiac coil. Images were acquired in the short axis plane at basal, mild and apical ventricular levels. An ECG-triggered segmented k-space fast gradient echo sequence with spatial modulation of magnetization was performed with the following parameters: grid tag spacing: 8 mm; echo time=2.54 ms; repetition time=48 ms; number of frames: 20-25 (depending of heart rate); pixel size:1.8 $\times$ 1.4 $\times$ 7 mm; bandwidth 446 Hz/pixel; flip angle: 10^o; acquisition time: 19 seconds (during one breathhold).

We performed a leave-one-out cross validation on the whole dataset. We employed Fast-PD algorithm [8] to perform MAP-MRF inference, which leads to a computational time of 0.781 second for segmenting an image on the average. For all the images in the dataset, we used the same parameters and the same initialization (see the two green circles in Fig. 4(a)). Satisfactory segmentation results on six test images from different sequences of different patients are presented in Fig. 3, which shows that our shape model can represent well the contraction of myocardium during the cardiac cycle and can deal with different scales of the myocardium boundaries. On the other hand, Fig. 4 shows the results obtained by giving different initializations with respect to the location and scale on the same test image. The consistent results demonstrate the robustness of our method with respect to the initialization.

For both quantitative evaluation and comparison purposes, we present in Fig. 5 the distributions of the Dice coefficients of the segmentation results for Ω_e (Fig. 5(a)), Ω_o (Fig. 5(b)) and Ω_m (Fig. 5(c)). Each sub-figure of Fig. 5 contains three boxes which present the Dice coefficients obtained by our method, the method in [7] and standard ASM method, respectively. Note that a higher Dice coefficient implies a better segmentation performance. Therefore, the obtained Dice coefficients demonstrate that our segmentation approach performs signficantly better than the other two methods. In particular, the better performance with respect to [7] demonstrates the power of the exact factorization of the regional data likelihood in the MRF. To conclude, our method performed well consistently throughout the experiments.

5. CONCLUSION

In this paper, we have proposed a novel approach for tagged cardiac MR image segmentation. The pairwise MRF which combines both the deformable shape priors and the exact inte-

gration of multi-dimensional regional/boundary statistics, and together with the Gabor features, leads to promising results that clearly outperform the prior art.

In the near future, we will deal with 3D tagged MR image segmentation and tracking with fusion of temporal prior, which is the most natural extension. Furthermore, we will extend this framework to implicitly account for scale variations. Last, but not least, the integration of visual support with anatomical landmark extraction to improve segmentation is a natural future direction of our research.

Appendix: Efficient regional data term computation

We present the numeric computation of regional data term $E^{(1)}_{\text{data}}(\mathbf{I}, \mathbf{\Omega}(\mathbf{u}))$ (Eq. 15). Let us consider the computation of the integral of $G^{(1)}(x, y)$ along a segment $\overrightarrow{u_a u_b}$ with the extremities $u_a = (x_a, y_a)$ and $u_b = (x_b, y_b)$. We first split the line segment into sub-pixel fragments. The extremities of the sub-pixel fragments are interpolated on $\overrightarrow{u_a u_b}$ by computing its intersections with the pixel grid, so that each fragment lies on a unit pixel square. Let $u_i = (x_i, y_i)$ and $u_{i+1} = (x_{i+1}, y_{i+1})$ be the extremities of a sub-pixel fragment $\overrightarrow{u_i u_{i+1}} \subset \overrightarrow{u_a u_b}$, we have

$$\begin{aligned} k \leq x_i, x_{i+1} \leq k+1 \\ l \leq y_i, y_{i+1} \leq l+1 \end{aligned} \tag{18}$$

k and l are integers.

Using the nearest neighbor interpolation to the likelihood images, the function $f(x, y) = \frac{\partial G^{(1)}(x,y)}{\partial x} = \log \frac{p_m(I(x,y))}{p_e(I(x,y))}$ is constant within each unit square region corresponding to a pixel. Thus $G^{(1)}$ is linear within each pixel and it can be rewritten as:

$$G^{(1)}(x, y) = \sum_{u=0}^{\lfloor x \rfloor - 1} f(u, \lfloor y \rfloor) + (x - \lfloor x \rfloor) f(\lfloor x \rfloor, \lfloor y \rfloor) \tag{19}$$

And then we can easily calculate the integral over the sub-pixel fragment $\overrightarrow{u_i u_{i+1}}$.

$$\int_{\overrightarrow{u_i u_{i+1}}} G^{(1)}(x(y), y) dy = (y_{i+1} - y_i) G^{(1)}(x_{c_i}, y_{c_i}) \tag{20}$$

while $x_{c_i} = \frac{x_i + x_{i+1}}{2}, y_{c_i} = \frac{y_i + y_{i+1}}{2}$ are the positions of the center point between the two extremities u_i and u_{i+1}.

We do the same computation process for the line integral of function $G^{(2)}$. Furthermore, we build two images to store the functions $G^{(1)}$ and $G^{(2)}$ after obtaining the likelihood images $\log \frac{p_m(I(x,y))}{p_e(I(x,y))}$ and $\log \frac{p_b(I(x,y))}{p_m(I(x,y))}$. In such a way, the data term energy can be computed efficiently.

6. REFERENCES

[1] T.S. Denney Jr, "Estimation and detection of myocardial tags in MR image without user-defined myocardial contours," *IEEE Transactions on Medical Imaging*, vol. 18, no. 4, pp. 330–344, 2002.

[2] Z. Qian, D. Metaxas, and L. Axel, "A learning framework for the automatic and accurate segmentation of cardiac tagged MRI images," *Computer Vision for Biomedical Image Applications*, pp. 93–102, 2005.

[3] A. Montillo, D. Metaxas, and L. Axel, "Automated model-based segmentation of the left and right ventricles in tagged cardiac MRI," *Medical Image Computing and Computer-Assisted Intervention (MICCAI)*, pp. 507–515, 2003.

[4] A. Bernardino and J. Santos-Victor, "Fast IIR isotropic 2-D complex Gabor filters with boundary initialization," *IEEE Transactions on Image Processing*, vol. 15, no. 11, pp. 3338–3348, 2006.

[5] S. Mallat, *A Wavelet Tour of Signal Processing, Third Edition: The Sparse Way*.

[6] T.F. Cootes, C.J. Taylor, D.H. Cooper, J. Graham, et al., "Active shape models-their training and application," *Computer Vision and Image Understanding*, vol. 61, no. 1, pp. 38–59, 1995.

[7] A. Besbes, N. Komodakis, G. Langs, and N. Paragios, "Shape priors and discrete MRFs for knowledge-based segmentation," *IEEE Conference on Computer Vision and Pattern Recognition (CVPR)*, pp. 1295–1302, 2009.

[8] N. Komodakis, G. Tziritas, and N. Paragios, "Performance vs computational efficiency for optimizing single and dynamic MRFs: Setting the state of the art with primal-dual strategies," *Computer Vision and Image Understanding*, vol. 112, no. 1, pp. 14–29, 2008.

[9] N. Paragios and R. Deriche, "Geodesic active regions and level set methods for supervised texture segmentation," *International Journal of Computer Vision*, vol. 46, no. 3, pp. 223–247, 2002.

[10] C. Fraley and A.E. Raftery, "How many clusters? Which clustering method? Answers via model-based cluster analysis," *The Computer Journal*, vol. 41, no. 8, pp. 578, 1998.

[11] V. Kolmogorov, "Convergent tree-reweighted message passing for energy minimization," *IEEE Transactions on Pattern Analysis and Machine Intelligence*, pp. 1568–1583, 2006.

[12] B. Glocker, N. Komodakis, G. Tziritas, N. Navab, and N. Paragios, "Dense image registration through MRFs and efficient linear programming," *Medical Image Analysis*, vol. 12, no. 6, pp. 731–741, 2008.